Science of the Total Environment 948 (2024) 174872

Contents lists available at ScienceDirect

Science of the Total Environment

journal homepage: www.elsevier.com/locate/scitotenv

Elucidating bacterial coaggregation through a physicochemical and imaging surface characterization

Ana C. Afonso [a,b,c,d], Jack Botting [e,f], Inês B. Gomes [a,b], Maria J. Saavedra [c], Lúcia C. Simões [d], Jun Liu [e,f], Manuel Simões [a,b,*]

[a] LEPABE - Laboratory for Process Engineering, Environment, Biotechnology and Energy, Faculty of Engineering, University of Porto, Rua Dr Roberto Frias, 4200-465 Porto, Portugal
[b] ALiCE - Associate Laboratory in Chemical Engineering, Faculty of Engineering, University of Porto, Rua Dr Roberto Frias, 4200-465 Porto, Portugal
[c] CITAB, Department of Veterinary Sciences, University of Trás-os-Montes e Alto Douro, 5000-801 Vila Real, Portugal
[d] CEB-LABBELS, University of Minho, Campus de Gualtar, 4710-057 Braga, Portugal
[e] Department of Microbial Pathogenesis, Yale School of Medicine, New Haven, CT 06536, United States
[f] New Haven Microbial Sciences Institute, Yale University, West Haven, CT 06516, United States

HIGHLIGHTS

- The coaggregation mechanism lacks a comprehensive understanding.
- Integrating physicochemical and imaging analyses reveals coaggregation dynamics.
- Unique surface properties dictate *D. acidovorans* coaggregation.
- Advanced imaging confirms the key role of pili-like adhesins in coaggregation.
- Known coaggregation aids in exploring biofilm formation and biotech applications.

GRAPHICAL ABSTRACT

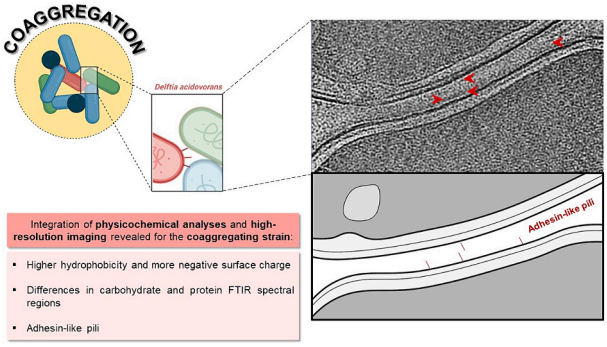

ARTICLE INFO

Editor: Damià Barceló

Keywords:
Cell-cell interaction
Co-adhesion energy
Cryo-electron tomography
Delftia acidovorans
FTIR
XDLVO theory

ABSTRACT

Bacterial coaggregation is a highly specific type of cell-cell interaction, well-documented among oral bacteria, and involves specific characteristics of the cell surface of the coaggregating strains. However, the understanding of the mechanisms promoting coaggregation in aquatic systems remains limited. This gap is critical to address, given the broad implications of coaggregation for multispecies biofilm formation, water quality, the performance of engineered systems, and diverse biotechnological applications. Therefore, this study aims to comprehensively characterize the cell surface of the coaggregating strain *Delftia acidovorans* 005P, isolated from drinking water, alongside a non-coaggregating strain, *D. acidovorans* 009P. By analyzing two strains of the same species, we aim to identify the factors contributing to the coaggregation ability of strain 005P. To achieve this, we employed a combination of physicochemical characterization, Fourier-transform infrared spectroscopy (FTIR), and advancing imaging techniques [transmission electron microscopy and cryo-electron tomography (cryo-ET)]. The

* Corresponding author at: LEPABE, Department of Chemical Engineering, Faculty of Engineering, University of Porto, Rua Dr. Roberto Frias, s/n, 4200-465 Porto, Portugal.
E-mail address: mvs@fe.up.pt (M. Simões).

https://doi.org/10.1016/j.scitotenv.2024.174872
Received 20 May 2024; Received in revised form 10 July 2024; Accepted 16 July 2024
Available online 20 July 2024

coaggregating strain (005P) exhibited higher surface hydrophobicity, negative surface charge, and cell surface and co-adhesion energies than the non-coaggregating strain (009P). The chemical characterization of bacterial surfaces through FTIR revealed subtle differences, particularly in spectral regions linked to carbohydrates and phosphodiesters/amide III of proteins (860–930 cm^{-1} and 1212–1240 cm^{-1}, respectively). Cryo-ET highlighted significant differences in pili structures between the strains, such as variations in length, frequency, and arrangement. The pili in the 005P strain, identified as pili-like adhesins, serve as key mediators of coaggregation. By integrating physicochemical analyses and high-resolution imaging techniques, this study conclusively links the coaggregation ability of *D. acidovorans* 005P to its unique pili characteristics, emphasizing their crucial role in microbial coaggregation in aquatic environments.

1. Introduction

In natural aquatic environments, bacterial cells are commonly found in close association with wet surfaces and interfaces in the form of biofilms (Romaní et al., 2016), where interspecies interactions can shape the development, structure and function of these communities (Burmølle et al., 2014; Elias and Banin, 2012; Rendueles and Ghigo, 2012; Yang et al., 2011). Such interactions may influence the growth and survival of the biofilm community (Peters et al., 2012). Coaggregation, a highly specific type of cell-cell interaction, has been suggested to be involved in the development of multispecies biofilms (Rickard et al., 2003a). Studies have indicated that coaggregation primarily occurs due to interactions between specific adhesive proteins, known as adhesins, located on the surface of bacterial cells (Niemann et al., 2004). These adhesins recognize and bind to specific receptor molecules, which contain complex sugars, on the surface of other bacterial cells (Katsikogianni et al., 2004). However, while this adhesin-receptor mechanism is well-documented for oral bacteria, knowledge in this field for aquatic bacteria is significantly lagging (Afonso et al., 2021). Therefore, understanding the surface properties of coaggregating strains from other environments than oral cavities is on demand.

The study of coaggregation in aquatic systems is crucial due to its wide range of implications for both natural ecosystems and engineered water systems. In natural aquatic environments, coaggregation influences the formation and stability of biofilms, which are essential for nutrient cycling, pollutant degradation, and maintaining ecological balance (Katharios-Lanwermeyer et al., 2014). These biofilms provide habitats for diverse microbial communities, supporting biodiversity and ecosystem health (Rickard et al., 2003b). In engineered systems, such as drinking water distribution systems (DWDS), coaggregation can negatively impact system performance and water quality, as well as facilitate the incorporation of pathogens into biofilms. Previous research has demonstrated that *Acinetobacter calcoaceticus* can act as a bridging bacterium, facilitating intergeneric coaggregation among DW bacteria (Simões et al., 2008). This ability to bridge different species enhances the formation and stability of biofilms, complicating efforts to manage biofouling and ensure the microbiological safety of DW. Moreover, the presence of *A. calcoaceticus* in DWDS can lead to more robust biofilms, which have higher resistance to standard disinfection methods, thus compromising water safety (Simões et al., 2010). Another study, examining various bacterial strains isolated from a model laboratory DWDS, revealed that biofilms with higher bacterial diversity were more resistant to chlorine-based disinfection (Simões et al., 2010). This finding underscores the importance of understanding the specific interactions and coaggregation behaviours among different bacterial species to develop more effective strategies for biofilm control and water treatment. Additionally, insights into coaggregation can enhance biotechnological applications, such as the development of biofilms for bioremediation of contaminated water bodies, and improving the degradation of organic pollutants and heavy metals (Malik et al., 2003). Therefore, studying coaggregation in aquatic systems is key to advancing environmental sustainability, public health, and industrial efficiency. In a recent study, *Delftia acidovorans* 005P, isolated from DW, demonstrated its ability to coaggregate and provide metabolic opportunities for other biofilm species, thereby creating a functional, cooperative microbial community (Afonso et al., 2023). Similar to what occurs in oral environments, the coaggregation ability of *D. acidovorans* 005P appears to be mediated by saccharides and/or proteins present on the cell surface (Afonso et al., 2023). However, other cell surface properties, including the presence of extracellular appendages, are important and may provide a competitive advantage for a microorganism where a multispecies community exists (Donlan, 2002). Therefore, it is important to study and understand how the cell surface properties of a coaggregating bacteria influence or determine coaggregation ability. So far, only a limited number of studies have been published on the influence of physicochemical surface properties on coaggregating bacteria, exclusively focused on the oral microbiome (Bos et al., 1994; Handley et al., 1987; Jenkinson, 1992).

This study performed a physicochemical characterization of *D. acidovorans* 005P surface to understand the mechanistic aspects involved in coaggregation within DW strains. *D. acidovorans* 009P strain, which lacks coaggregation ability, was studied for comparison. Additionally, transmission electron microscopy (TEM) and cryo-electron tomography (cryo-ET) were used to take a closer view of the bacterial surface and its structures. TEM enables high-resolution imaging of thin sections of biological specimens, allowing for detailed visualization of cellular structures at the nanoscale (Malatesta, 2021). It utilizes a beam of electrons transmitted through the specimen to create detailed images with exceptional clarity (Malatesta, 2021). On the other hand, cryo-ET takes imaging to the next level by allowing three-dimensional reconstructions of frozen-hydrated specimens (Baumeister, 2022). This technique is particularly valuable for studying dynamic cellular processes and interactions in their native state (Dunstone and de Marco, 2017). The ability of Cryo-ET to capture detailed structural information while preserving the native state of the specimen makes it an invaluable tool for investigating complex biological phenomena *in situ* (Baumeister, 2022). This combination of physicochemical analysis and high-resolution imaging techniques has a remarkable potential to reveal new details about the molecular structures and mechanisms involved in bacterial coaggregation in aquatic systems.

2. Methods

2.1. Bacterial cell growth and preparation

Two *D. acidovorans* strains isolated from DW and with different coaggregation abilities (Afonso et al., 2023) were selected for the characterization of the cell surface. The experimental setup is illustrated in Fig. 1. Both strains are deposited in the publicly accessible culture collection MUM (Micoteca da Universidade do Minho, Braga, Portugal) with accession codes MUM 24.11 (*D. acidovorans* 005P) and MUM 24.12 (*D. acidovorans* 009P). Bacterial cells were grown overnight in R2A broth [peptone 05 g L^{-1} (Oxoid, UK), glucose 0.5 g L^{-1} (Chem-Lab, Belgium), magnesium sulfate heptahydrate 0.1 g L^{-1} (Merck, Germany), sodium pyruvate 0.3 g L^{-1} (Merck, Germany), yeast extract 0.5 g L^{-1} (Merck, Germany), casein hydrolysate 0.5 g L^{-1} (Oxoid, UK), starch soluble 0.5 g L^{-1} (Sigma-Aldrich, Portugal) and di-potassium phosphate trihydrate 0.4 g L^{-1} (Aplichem Panreac, USA)], at room temperature

(23 °C ± 2), under agitation (150 rpm). Then, cells were harvested by centrifugation (10 min, 3100 ×*g*), washed three times in saline solution (NaCl 8.5 g L^{-1}) and resuspended in ultrapure water at a concentration of 1 × 10^8 CFU mL^{-1}.

2.2. Surface contact angle measurements

Bacterial suspensions were filtered using a sterile cellulose nitrate membrane filter, pore size 0.45 μm, 47 mm diameter (Sartorius, Thermo Fisher, Portugal) to achieve a uniform layer of microorganisms. The surface tension of bacteria was determined through the sessile drop contact angle method. Contact angles were determined as described by Simões et al. (2007) at room temperature using three different liquids: two polar (water and formamide) and one apolar (α-bromonaphtalene) (Sigma, Portugal). Determination of contact angles (in degrees) was performed automatically using a model OCA 15 Plus (DATAPHYSICS, Germany) video-based optical contact angle measure instrument, allowing image acquisition and data analysis. Contact angle measurements (at least 25 determinations) were performed in three independent experiments. The reference liquids' surface tension components were obtained from the literature (Janczuk et al., 1993).

2.3. Surface hydrophobicity

The surface hydrophobicity was determined based on contact angle data as proposed by van Oss et al. (1989). According to the extended Young equation (Eq. (1)), the contact angles (θ) of a liquid (*L*) on a surface are related to the total surface tension (γ, mJ m^{-2}), which can be separated into two components: apolar (γ^{LW}) and polar (γ^{AB}), with $\gamma_L = \gamma^{LW} + \gamma^{AB}$ and $\gamma^{AB} = 2\sqrt{\gamma^+\gamma^-}$. Where γ^+ and γ^- are the electron-acceptor and electron-donor parameters, respectively.

$$(1+cos\theta)\gamma_L = 2\left(\sqrt{\gamma_L^{LW}} + \sqrt{\gamma_L^+\gamma^-} + \sqrt{\gamma_L^-\gamma^+}\right) \quad (1)$$

The degree of hydrophobicity (ΔG_{iwi}) was expressed as the free energy of interaction between two identical entities (*i*) when immersed in water (*w*), as the sum of Liftshitz-van der Waals (*LW*) and Lewis acid-base (*AB*) interaction free energies (Eq. (2)). The *LW* component includes London dispersion forces, Debye induction (dipole-induced dipole) and Keesom orientation (dipole-dipole) interactions. *AB* interactions include electron donor (γ^-) and electron acceptor (γ^+) contributions, thus accounting for hydrogen bonding and p-electron interactions too (Janczuk et al., 1993). Thermodynamically, for $\Delta G_{iwi} <$ 0 mJ m^{-2}, the bacterial surface is considered hydrophobic, whereas the bacterial surface is considered hydrophilic for $\Delta G_{iwi} > 0$ mJ m^{-2} (Borges et al., 2012).

$$\Delta G_{iwi} = \Delta G_{iwi}{}^{LW} + \Delta G_{iwi}{}^{AB} = -2\gamma_{iw}^{LW} - 2\gamma_{iw}^{AB} \quad (2)$$

where,

$$\gamma_{iw}^{LW} = \left(\sqrt{\gamma_i^{LW}} - \sqrt{\gamma_w^{LW}}\right) \text{ and } \gamma_{iw}^{AB} = 2\left(\sqrt{\gamma_i^+\gamma_i^-} + \sqrt{\gamma_w^+\gamma_w^-} - \sqrt{\gamma_i^-\gamma_w^+} - \sqrt{\gamma_i^-\gamma_w^+}\right).$$

2.4. Cell surface energy and co-adhesion energy

The cell surface energy (SE) of the bacterial cells was determined based on the water contact angle results. The cell SE can affect the co-adhesion energy of cells (ΔF_{co-adh}), which can be expressed as follows (Bos et al., 1999):

$$\Delta F_{co-adh} = \gamma^{bb} - 2\gamma^{bl} \quad (3)$$

where γ^{bb} and γ^{bl} are the interfacial energies of the bacterial cell-bacterial cell interface and bacterial cell-liquid interface, respectively. Using Neumann's equation of state (Eq. (4)), $\Delta F_{co-adh} = \gamma^{bb}$ can be expressed as (Eq. (5)):

$$\gamma^{ml} = \gamma^{mv} + \gamma^{lv} - 2\sqrt{\gamma^{mv}\gamma^{lv}}e^{-\beta\left(\gamma^{lv}-\gamma^{mv}\right)^2} \quad (4)$$

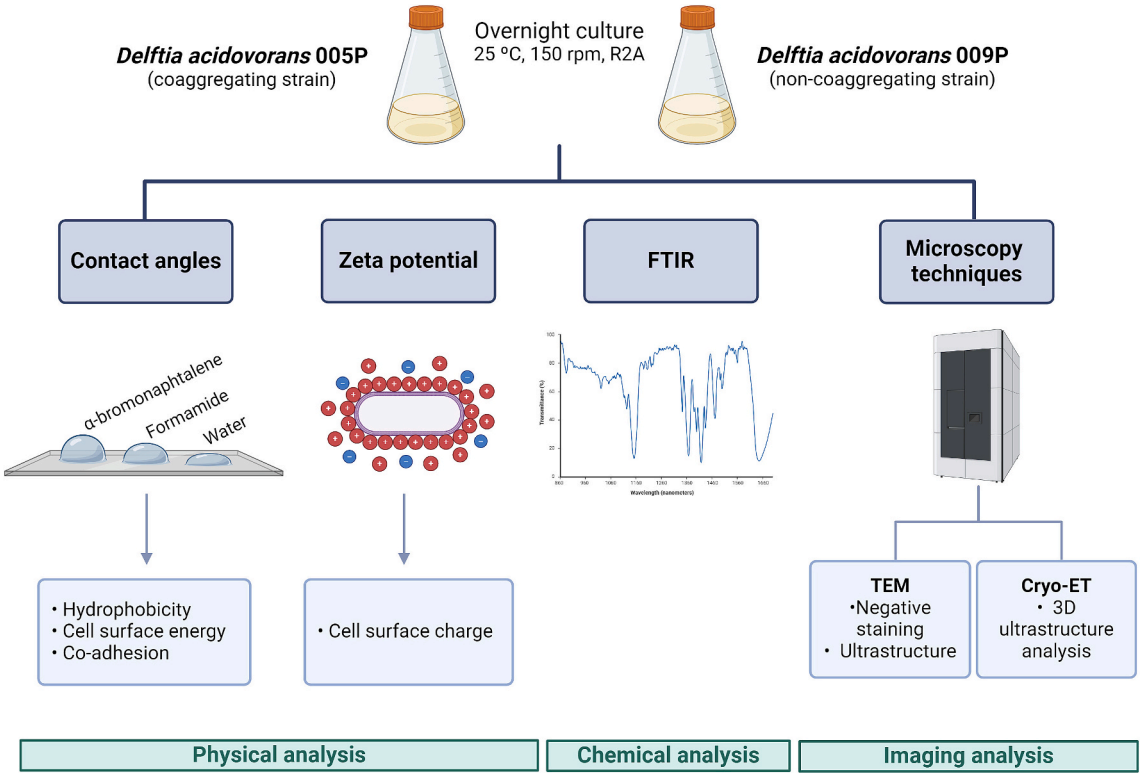

Fig. 1. Experimental setup for characterizing the cell surface of *D. acidovorans* 005P (coaggregating) and *D. acidovorans* 009P (non-coaggregating). Created with BioRender.com.

$$\Delta F_{co-adh} = 4\sqrt{\gamma^{bv}\gamma^{lv}}e^{-\beta\left(\gamma^{lv}-\gamma^{bv}\right)^2} - 2\gamma^{bv} - 2\gamma^{lv} \quad (5)$$

where γ^{bv} is the cell SE. γ^{lv} is the surface tension of the culture medium. Because the culture medium is generally water-based, γ^{lv} can be regarded as the surface tension of water (72.8 mJ m^{-2}). The value of β was experimentally determined to be 0.0001247 (mJ m^{-2})$^{-2}$ (Neumann et al., 2010).

2.5. Zeta potential measurements

The zeta potential is an electrochemical property that describes the bacterial surface charge and provides useful information about cell surface characteristics (Halder et al., 2015). First, bacterial cells were prepared as described before (Section 2.1). Then, the measurements of the zeta potential (ζ) of bacterial cells were performed using a Zetasizer PRO Blue electrophoretic light scattering spectrophotometer (Malvern Instruments, UK). The electrophoretic mobility (μ_e) at an applied voltage of 150 V and a temperature of 22 °C, were then converted to zeta potential using the Helmholtz von Smoluchowski relation (Eq. (6)), where $\varepsilon\varepsilon_0$ corresponds to the dielectric permittivity and η to the viscosity of the suspending solution (Bayoudh et al., 2009). The experiments were performed in triplicate.

$$\mu_e = \frac{\varepsilon\varepsilon_0}{\eta}\zeta \quad (6)$$

2.6. FTIR-ATR spectral acquisition

Fourier transform infrared (FTIR) spectra were acquired using a PerkinElmer Spectrum BX FTIR spectrophotometer equipped with a deuterated triglycine sulfate (DTGS) detector and a PIKE Technologies Gladi attenuated total reflection (ATR) accessory from 4000 to 600 cm^{-1} with a resolution of 4 cm^{-1} and 16 scan co-additions. Briefly, bacterial cells were grown on Mueller-Hinton agar for 16 h at 37 ± 2 °C to avoid spectral interferences due to the age of the colony. The colonies were directly transferred from the agar plates to the ATR crystal and air-dried to obtain a thin film. Three instrumental replicates and three biological replicates were acquired and analysed for each strain, corresponding to a minimum of nine spectra per strain (Sousa et al., 2013; Sousa et al., 2014a, 2014b). Spectra were pre-processed using methods previously optimized for other bacterial species, to minimize variation related to spectrum acquisition and maximize differences between spectra (Rodrigues et al., 2020; Sousa et al., 2014a, 2014b).

2.7. Transmission electron microscopy

To unravel the cellular details of both *D. acidovorans* strains at higher resolution, TEM was applied to visualize the ultrastructural features of the bacterial strains (Malatesta, 2021). *D. acidovorans* suspensions were prepared as referred to in Section 2.1. For ultrastructure analysis, samples were fixed with 2.5 % glutaraldehyde and 2 % paraformaldehyde in 0.1 M sodium cacodylate buffer (pH 7.4) solution for 2 days. After that, cell suspensions were washed in 0.1 M sodium cacodylate buffer, and embedded in Histogel™ (Thermo, HG-4000-012). Cell blocks were washed with the same buffer and post-fixed by incubation for 2 h in 2 % osmium tetroxide in 0.1 M sodium cacodylate buffer (pH 7.4) solution. Then, cell blocks were washed using the same buffer and incubated with 1 % uranyl acetate overnight. After washing in 0.1 M sodium cacodylate buffer, samples were dehydrated in a gradient series of ethanol solutions (70 %, 80 %, 90 % and 100 % (v/v), for 10 min each) and embedded in Epon (EMS). Ultrathin sections were cut at 50 nm and prepared on RMC Ultramicrotome (PowerTome, USA) using a diamond knife and recovered to 200 mesh copper grids, followed by a double contrast method with 2 % uranyl acetate and saturated lead citrate solution. Visualization was performed at 80 kV in a JEOL JEM 1400 microscope (Japan), and digital images were acquired using a CCD digital camera Orious 1100 W (Tokyo, Japan). TEM was performed at the HEMS core facility at i3S, University of Porto, Portugal.

For negative staining, samples were adsorbed to glow-discharged carbon-coated collodion film on 400-mesh copper grids. Then, the grids were washed with deionized water and stained with 1 % uranyl acetate.

2.8. Cryo-electron tomography

To extend ultrastructure analysis further by enabling three-dimensional reconstructions of bacterial structures in their native and hydrated state, cryo-ET analysis was performed (Baumeister, 2022). Briefly, BSA gold tracers (Aurion, Wageningen, NL) of 10 nm were added to bacterial suspensions of *D. acidovorans* in phosphate buffer saline (PBS) ($OD_{600nm} \approx 1$). The mixtures were deposited onto cryo-electron microscopy (cryo-EM) grids (Quantifoil R2/1, Cu 200, Ted Pella, Inc., Redding, CA, USA) and rapidly plunge-frozen in liquid ethane (Liu et al., 2009). The frozen-hydrated specimens were visualized using a 300 kV Titan Krios electron microscope (Thermo Fisher Scientific, Waltham, MA, USA) equipped with a K3 summit direct detection camera and a BioQuantum energy filter (Gatan, Pleasanton, CA, USA). Tilt series were acquired at 19,500× magnification, with the stage tilted from −48° to +48° at 3° increments. Cryo-ET data alignment and reconstruction were performed using MotionCor2 for frame alignment (Zheng et al., 2017), and IMOD for gold tracer bead tracking and alignment (Kremer et al., 1996). The tomograms were reconstructed *via* the simultaneous iterative reconstruction technique (SIRT) (Cai et al., 2022). IMOD software was utilized for visualizing the tomographic reconstructions (Kremer et al., 1996).

2.9. Statistical analysis

Contact angles and zeta potential data analysis were performed using the statistical program SPSS version 27.0 (Statistical Package for the Social Sciences, USA). Descriptive statistic was used to calculate the mean and standard deviation (SD). The data was analysed using a paired sample *t*-test, since the variables were normally distributed, and were based on a confidence level ≥ 95 % ($P < 0.05$ was considered statistically significant). OriginPro 2023 software (OriginLab, USA) was used to acquire FTIR spectra and to perform principal component analysis (PCA - for dimensionality reduction and enhanced data visualization).

3. Results and discussion

3.1. The coaggregating strain has a more hydrophobic and negatively charged surface

D. acidovorans 005P and *D. acidovorans* 009P were characterized in terms of physical and chemical cell surface properties. Both *D. acidovorans* strains had a water contact angle lower than 65^0 and a $\Delta G_{iwi} > 0$ mJ/m^2, which means that both have hydrophilic surfaces (Table 1). However, the hydrophobicity values were significantly different ($P < 0.05$). Strain *D. acidovorans* 005P had the highest surface hydrophobicity value (36.6 mJ m^{-2}) while *D. acidovorans* 009P had the lowest (29.0 mJ m^{-2}). Other authors have already observed a large variation in the degree of hydrophobicity between strains of the same species (Min et al., 2006; Simões et al., 2007; Teixeira et al., 2005; van der Mei et al., 1998). The hydrophobicity of the bacterial cell surface can be established by several factors such as outer membrane proteins and lipids, S-layer proteins, various fimbriae or core oligosaccharides, lipopolysaccharides, and fimbrial adhesins (Higashi et al., 1998; Morath et al., 2005; Sidhu and Olsen, 1997; Zähringer et al., 1995). These differences have been previously observed for strains of *D. acidovorans* and may be related to the different surface properties of the bacterial cell wall, such as surface proteins (Simões et al., 2007). In a previous study, where the proteome of *D. acidovorans* 005P and 009P was characterized,

Table 1
Contact angles with water (θ_W), formamide (θ_F) and α-bromonaphthalene (θ_B), surface tension parameters (γ_b^{LW}, γ_b^{AB}, γ_b^+ and γ_b^-), free energy of interaction (ΔG_{iwi}), cell surface energy, co-adhesion energy and zeta potential of the *D. acidovorans* strains when immersed in water. Values are mean ± standard deviation of three independent experiments. *Statistically different values between strains.

D. acidovorans strains	Contact angle (°)			Surface tension parameters (mJ/m^2)				Hydrophobicity	SE (mJ/m^2)	Co-adhesion energy (mJ/m^2)	Zeta potential (mV)
	θ_W	θ_F	θ_B	γ_b^{LW}	γ_b^{AB}	γ_b^+	γ_b^-	ΔG_{iwi} (mJ/m^2)	γ^{bv}	ΔF_{co-adh}	ζ
005P	31.6 ± 3.4	39.4 ± 3.3	44,4 ± 5.9	31.9 ± 1.2	11.9 ± 0.9	0.7 ± 0.1	53.6 ± 0.8	36.6 ± 0.6*	125.7*	−127.4*	−46,8 ± 0,2*
009P	15.9 ± 0.7	20,4 ± 2.2	52.3 ± 4.5	29.1 ± 0.3	26.6 ± 0.6	3.3 ± 0.2	54.2 ± 0.4	29.0 ± 0.6*	118.7*	−97.4*	−44,6 ± 0,2*

differences were found in cell appendage proteins (Afonso et al., 2024). These findings help to support the differences in cell surface hydrophobicity observed in this study. The results further suggest a potential parallel with oral bacteria, indicating that proteins might play a role in the coaggregation of bacteria derived from aquatic systems as well. Handley et al. (Handley et al., 1987) showed that coaggregating oral bacteria had higher hydrophobicity than the non-coaggregating ones. Regarding the remaining physicochemical parameters, the apolar component (γ^{LW}) values were 29.1 mJ m^{-2} for *D. acidovorans* 009P and 31.9 mJ m^{-2} for *D. acidovorans* 005P. The non-coaggregating strain, *D. acidovorans* 009P, had the highest surface polar component (γ^{AB} = 26.6 mJ m^{-2}). The results further showed that both strains have a high electron donor character (γ^-), with low electron acceptor ability (γ^+). These results are in line with previous reports, revealing the genus *Delftia* with a high bacterial surface electron donor character (Simões et al., 2007; Yang et al., 2021).

The surface charge of both *D. acidovorans* strains was analysed in terms of zeta potential (Table 1). As a rule, most bacteria have a net negative surface charge that is balanced by oppositely charged counterions present in the surrounding medium (Halder et al., 2015). Here, the zeta potential values were −46.8 mV and −44.6 mV for *D. acidovorans* 005P and *D. acidovorans* 009P, respectively. A more negative zeta potential was observed for the coaggregating strain *D. acidovorans* 005P ($P < 0.01$). For the genus *Delftia*, values between −20 and −40 mV of zeta potential have already been observed (Yang et al., 2021). This range is related to the species tested and to the ionic strength of the solution in which the test was carried out. Thus, it can be considered that the values presented in this study are in line with those previously described (Yang et al., 2021). These differences in surface charges between both strains can be explained by the higher polar component ascribed to *D. acidovorans* 009P (Oh et al., 2018). Furthermore, any difference in cell surfaces that *a priori* would be similar (*i.e.*, same species), would lead to changes in the surface charge. For example, Tariq et al. (2012) observed that mutant strains of *Enterococcus faecalis* with under or overexpression of *Ebp* pili structural genes differed in zeta potential values. The difference observed between the zeta potential values of the two *D. acidovorans* strains might indicate differences in their cell surface profiles.

While physical analyses provide valuable insights into bacterial surface properties, they are limited in their ability to offer detailed molecular-level information (Kimkes and Heinemann, 2020). Therefore, incorporating chemical analyses like FTIR (Section 3.3) can provide a more nuanced understanding, mitigating the potential limitations of thermodynamic theories in characterizing bacterial surface interactions.

3.2. Higher co-adhesion energy can be a determinant of cell aggregation

The relationship between ΔF_{co-adh} and cell SE (γ^{bv}) was analysed, proving a higher SE value for *D. acidovorans* 005P (SE = 125.7 mJ m^{-2}) than for *D. acidovorans* 009P (SE = 118.7 mJ m^{-2}) ($P < 0.05$). The increase of SE provides more negative co-adhesion energy and indicates an increase in cell-cell interaction. It means that, when the cell has a high SE, the co-adhesion energy between the cells is high, which can thus increase cell aggregation. Co-adhesion energy is expected to serve as an indicator of bacterial coaggregation since both phenomena are closely related. Co-adhesion predominantly involves the interaction between suspended cells and those already adhered to the substrate, while aggregation occurs between cells in suspension or between bacterial cells in suspension and specific bacterial counterparts (*i.e.* bridging bacteria) that colonize a biofilm (Afonso et al., 2021; Katharios-Lanwermeyer et al., 2014; Kolenbrander et al., 2006; Rickard et al., 1999).

Previous studies have suggested that bacterial coaggregation contributes to the development of biofilms by two routes (Bos et al., 1994; Busscher et al., 1995): i) single cells in suspension adhere specifically to genetically distinct cells in the developing biofilm; or, ii) previously formed coaggregates in suspension adhere to the developing biofilm. In both cases, bacterial cells in suspension specifically adhere to biofilm cells by co-adhesion (Rickard et al., 2003a). Therefore, we propose that by determining the co-adhesion energy for various coaggregating strains, we will be able to define a value from which the ability to coaggregate exists. Co-adhesion of oral bacteria was previously studied using a quantitative method, and a difference in co-adhesion behaviour between coaggregating and non-coaggregating strains was also observed (Bos et al., 1994). However, to our knowledge, this is the first study that resorts to the use of a thermodynamic theory to assess the co-adhesion energy between bacterial cells. Zhang et al. (2020) have already applied this theory to assess co-adhesion between microalgae cells. Nevertheless, we do not believe that the results can be compared since the composition of the cell walls of bacteria and microalgae are different.

3.3. FTIR revealed differences in specific regions of proteins and carbohydrates

Various theoretical and thermodynamic theories have been used over the years to describe bacterial adhesion, mainly to solid surfaces (Bos et al., 1999; Janczuk et al., 1993; Neumann et al., 2010; van Oss et al., 1989). However, these theories ignore important biological factors such as the heterogeneity of the bacterial surface (Ojeda et al., 2008). FTIR spectroscopy has emerged as a more complete bacterial cell surface characterization technique, which is fundamental to understanding the interactions between cells and the environment, and for elucidating the mechanisms involved in bacterial transport, aggregation and biofilm formation (Eboigbodin et al., 2007; Ojeda et al., 2008). The FTIR-ATR spectra of *D. acidovorans* 005P and 009P are shown in Fig. 2. The FTIR-ATR spectra exhibited the typical infrared absorption bands of intact bacterial spectra: fingerprint region (900–600 cm^{-1}), polysaccharides (1185–900 cm^{-1}), mixed region of phospholipids/DNA/RNA (1500–1185 cm^{-1}), proteins/amides I and II (1700–1500 cm^{-1}) and lipids (3000–2800 cm^{-1}) (Maquelin et al., 2002; Naumann et al., 1991; Sousa et al., 2014a, 2014b). For multivariate analysis, PCA revealed three groups clustered separately, corresponding to the three

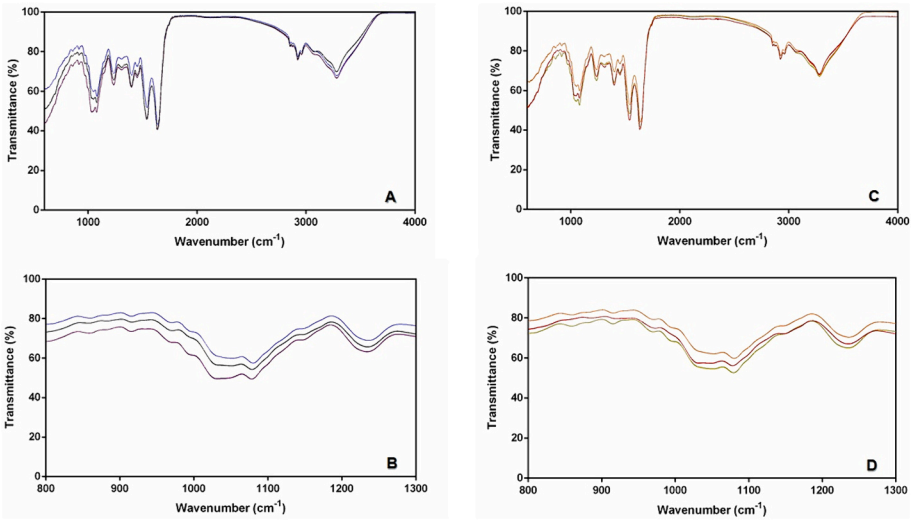

Fig. 2. *Delftia acidovorans* 005P (A, B) and 009P (C, D) FTIR-ATR spectra of three instrumental replicates and three biological replicates. Spectra (B) and (D) show in greater detail the region between 800 and 1000 cm^{-1} where small differences in bands corresponding to proteins and saccharides/carbohydrates were observed.

biological replicas. A high correlation between strains for each replicate was observed, where principal component 1 (PC1) and PC2 explained 87.9 % and 8.7 % of the variance, respectively (Fig. 3). Although the differences observed between the strains were not more significant than the differences observed between replicates of the same strain (Fig. 3), differences were encountered in bands corresponding to proteins and saccharides/carbohydrates (Fig. 2C and D).

The comparison between the spectra revealed differences in the 860–930 cm^{-1} and 1212–1240 cm^{-1} spectral regions, suggesting differences in chemical compounds related to carbohydrates and phosphodiesters/amide III of proteins, respectively (Meyers, 2006). Studies with a marine strain of *Pseudomonas* characterized the region 860–930 cm^{-1} as indicating the presence of sulfate ester - a sulfated carbohydrate (Tandavanitj and Okutani, 1989; Worawattanamateekul and Okutani, 1992). In fact, in marine environments, carbohydrate-carbohydrate interactions mediated by sulfate esters are involved in the aggregation of marine sponge cells (Spillmann et al., 1995; Vilanova et al., 2009, 2016). On the other hand, the role of sulfated carbohydrate-binding protein from *Lactobacillus reuteri* was demonstrated in bacterial adhesion to mucosal surfaces of the gastrointestinal tract of mammals (Nishiyama et al., 2013). Regarding the 1212–1240 cm^{-1} spectral region, a band at 1240 cm^{-1} is a marker of proteins and polypeptides with β-conformation (Maiti et al., 2004). In bacteria, the β-sheet conformation is usually found in amyloid structures (Van Gerven et al., 2015). *Fusobacterium nucleatum*, a known oral coaggregating bacteria, secretes an adhesin (FadA) with amyloid properties (Meng et al., 2021). It is unclear whether the FadA adhesin is involved in the *F. nucleatum* coaggregation mechanism. However, in a study evaluating the interaction between *Porphyromonas gingivalis* and *F. nucleatum* in the context of periodontitis, the authors highlighted the fundamental role of the FadA adhesin. The downregulation of FadA expression, attributed to proteases within *P. gingivalis*, highlighted the importance of specific adhesins, particularly FadA, in modulating bacterial coaggregation in oral environments (Zhang et al., 2022). Although previous proteomics studies have not identified this specific adhesin in any of the *D. acidovorans* strains (Afonso et al., 2024), other similar proteins should not be discarded.

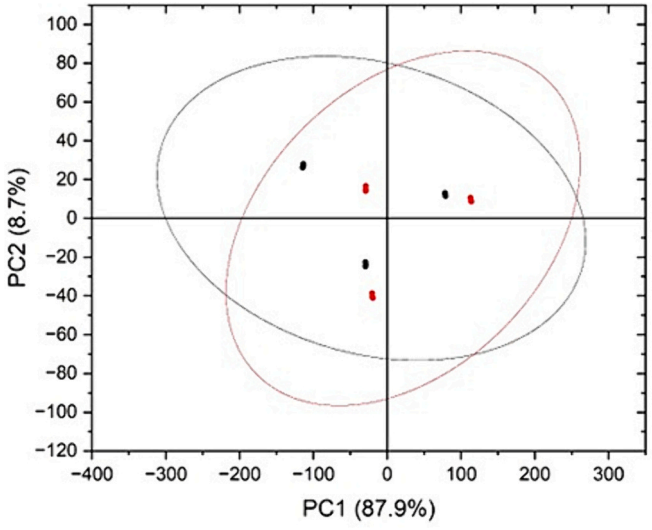

Fig. 3. Principal component analysis of *D. acidovorans* 005P (black) and 009P (red) established by analysis of average from 3 replicas of FTIR-ATR spectra. The ellipses represent 95 % confidence for both strains.

3.4. Cryo-ET reveals the presence of adhesin-like pili in the coaggregating strain

TEM revealed through negative staining that both strains have flagella (Fig. 4A and B). The ultrastructure analysis of sectioned samples showed the different layers of the cell envelope (Fig. 4C and D). Furthermore, there was a loss of cell appendages, namely flagella, and a deformation of the cell morphology during sample preparation, a known limitation of the technique (Ivanchenko et al., 2021). On the other hand, cryo-ET is a more preservative technique which minimizes artefacts associated with dehydration and chemical fixation and enhances the resolution of small features (Lučić et al., 2013). Moreover, cryo-ET enables capturing multiple tilted images around a single axis to reconstruct a detailed 3D representation of the specimen, allowing for more comprehensive and accurate visualization of small structures, such as adhesions (Baumeister, 2022; Dunstone and de Marco, 2017).

The cryo-ET reconstruction allowed us to visualize the cellular morphology of both strains and their structures (Fig. 4E and F). Similar to TEM analysis, both strains showed flagella (Fig. 4E and F). Pili filaments were also observed, and the length of the filaments was different between strains (Figs. 5 and 6). In the coaggregating strain (005P), these filaments were shorter than in the non-coaggregating strain (009P) and almost imperceptible, possibly attributable to adhesin-like pili (Fig. 6 and Movie 1). In a study on *Pseudomonas aeruginosa* cell-cell interactions, filaments like those observed here were revealed by cryo-ET,

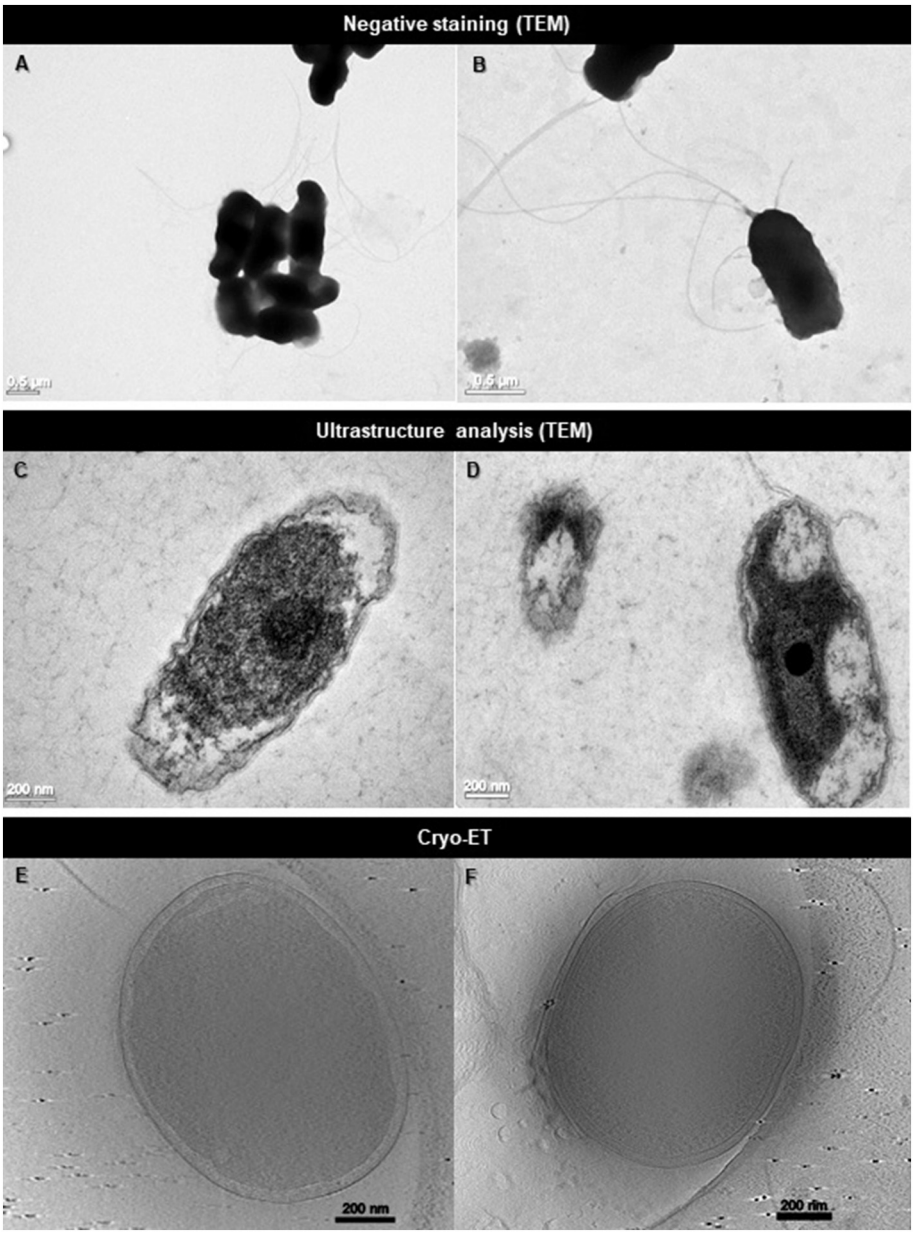

Fig. 4. Cell overview of *D. acidovorans* by three different approaches: TEM negative staining (A and B) ultrastructure analysis (C and D), and cryo-ET (E and F). Flagella were observed in both strains, but differences in morphology and cell envelope were not evident between the coaggregating (A, C and E) and non-coaggregating (B, D, F) strains.

and the authors confirmed them to be CdrA adhesins (Melia et al., 2021). In another study, the authors highlighted the critical role of pili length in the coaggregation of the oral colonizer *Actinomyces oris* (Chang et al., 2019). Using a *srtA*-deficient mutant, the authors observed that genetic disruption of *srtA* resulted in excessively long pili catalyzed by the pilus-specific sortase SrtC2, which interrupted interspecies interactions and coaggregation. By restoring SrtA, the length of the pili progressively shortened, reestablishing coaggregation (Chang et al., 2019). Another difference between coaggregating and non-coaggregating *D. acidovorans* is in the frequency and arrangement of pili along the cell surface. While in *D. acidovorans* 009P pili appear practically evenly distributed over the entire cell surface, in *D. acidovorans* 005P they are less frequent (≈3 per cell) and tend to appear in the closest location to other cells (Fig. 6). These filaments are exclusive to the coaggregating strain and correspond to the filaments identified as adhesins in coaggregating cells (Chang et al., 2019). Put together, these observations strongly suggest that these filaments are a major determining factor of coaggregation in *D. acidovorans*.

4. Conclusion

Our investigation into the surface physicochemical properties of two *D. acidovorans* strains revealed significant differences that clarify the mechanisms underlying coaggregation. Variations in hydrophobicity and cell surface charge were observed, indicating changes in protein expression likely related to cellular appendages. FTIR spectroscopy confirmed these findings by showing distinct differences in the protein and carbohydrate regions on the bacterial cell surface. Furthermore, the observed differences in pili between strains markedly affect their coaggregation ability. Cryo-ET revealed pili-like adhesins on the surface of the coaggregating 005P strain, predominantly appearing in areas near other cells, implying their expression is triggered by cell-cell contact or proximity. In contrast, the non-coaggregating strain displayed long pili distributed across the entire cell surface. Additionally, our novel

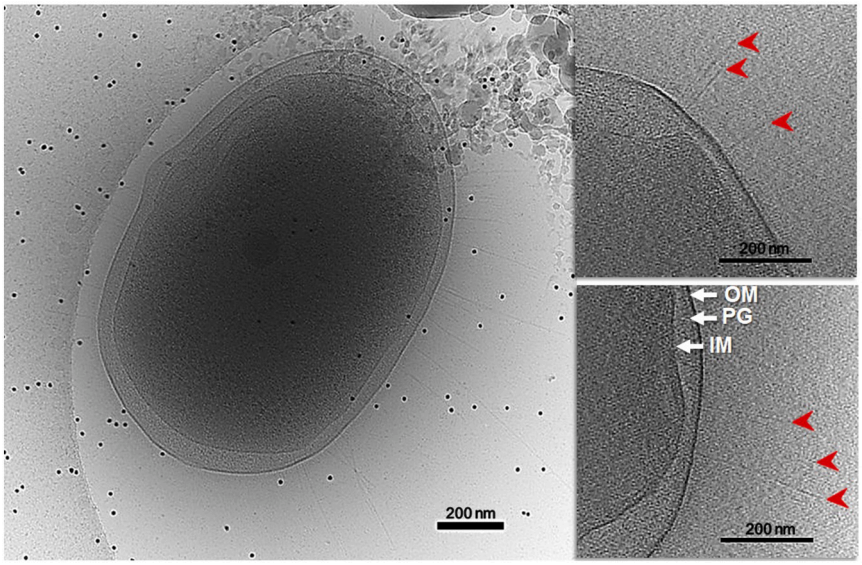

Fig. 5. Long pili (white dashed boxes) were revealed on the non-coaggregating *D. acidovorans* 009P strain by cryo-EM (big panel) and cryo-ET (red arrowheads). The white arrows indicate the outer membrane (OM), peptidoglycan layer (PG) and inner membrane (IM).

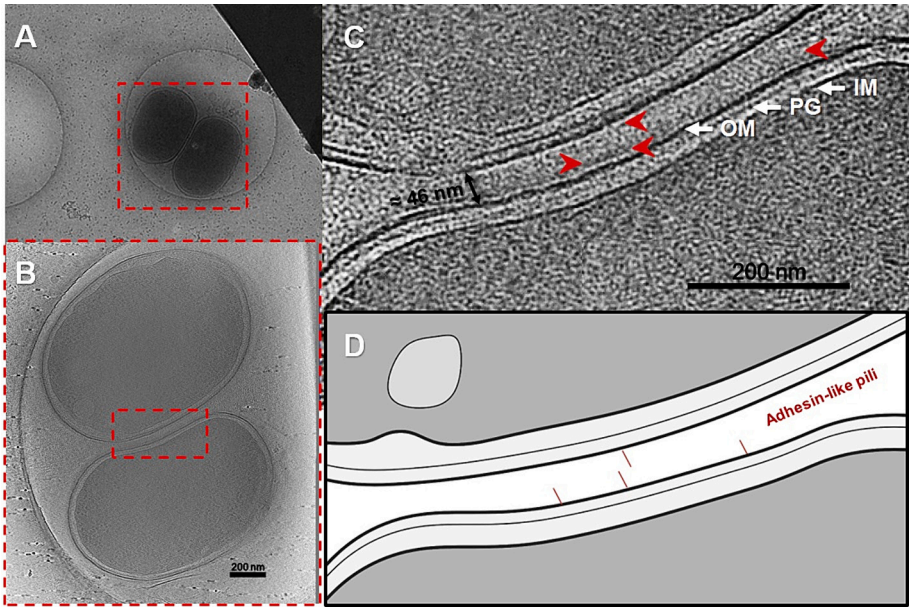

Fig. 6. Ultrastructure from the 3-D reconstruction of *D. acidovorans* 005P (coaggregating strain) shows short adhesin-like pili in the cellular interface. Cryo-EM grid montage (A) and the tomogram slice (B) show two nearby cells. (C) is an enlarged view of the boxed region in (B), being the adhesins highlighted with red arrowheads. (D) shows adhesin-type pili at the interface of the two cells as seen in (C). The white arrows indicate the outer membrane (OM), peptidoglycan layer (PG) and inner membrane (IM).

examination of co-adhesion energy provided insights into bacterial coaggregation potential, suggesting a correlation between surface energy and cell-cell interaction.

In summary, our study underscores the critical importance of comprehending the physicochemical properties and ultrastructural characteristics of the cell surface in understanding bacterial coaggregation mechanisms. Subtle differences between strains dictate their ability to coaggregate, highlighting the need for further research into the genetic basis of these phenotypic variations. These findings have important implications for both microbial ecology and water treatment, as understanding these interactions can enhance the development of targeted microbial consortia for biofilm engineering, optimize water treatment processes, and improve bioremediation efforts.

Supplementary data to this article can be found online at https://doi.org/10.1016/j.scitotenv.2024.174872.

Funding

This work was financially supported by: Project InnovAntiBiofilm (ref. 101157363) financed by European Commission (Horizon-Widera 2023-Acess-02/Horizon-CSA); LEPABE, UIDB/00511/2020 (DOI: 10.54499/UIDB/00511/2020) and UIDP/00511/2020 (DOI: 10.54499/UIDP/00511/2020), and ALiCE, LA/P/0045/2020 (DOI: 10.54499/LA/P/0045/2020), funded by national funds through FCT/MCTES (PIDDAC); CEB, UIDB/04469/2020 (DOI: 10.54499/UIDB/04469/2020) and by LABBELS – Associate Laboratory in Biotechnology,

Bioengineering and Microelectromechanical Systems, LA/P/0029/2020; CITAB, UIDB/04033/2020 (DOI: 10.54499/UIDB/04033/2020); the FCT contract attributed to I.B.G (2022.06488.CEECIND) and the FCT PhD grant attributed to A.C.A (DOI: 10.54499/2020.04773.BD). J.B. and J.L. are supported by grants R01AI087946 and R01AI132818 from the National Institute of Allergy and Infectious Diseases (NIAID); cryo-ET data were collected at Yale CryoEM Resource funded in part by the NIH grant 1S10OD023603-01A1. The authors acknowledge the support of the CIQUP – Centro de Investigação em Química da Universidade do Porto (Prof. Fernanda Borges) in the zeta potential measurements; the UCIBIO – Applied Molecular Biosciences Unit of the Faculty of Pharmacy of the University of Porto (Prof. Luísa Peixe, Dr. Filipa Grosso and Dr. Ângela Novais) for the FTIR spectra acquisition; and the i3S Scientific Platform Histology and Electron Microscopy (HEMS), member of the PPBI (PPBI-POCI-01-0145-FEDER-022122).

CRediT authorship contribution statement

Ana C. Afonso: Writing – original draft, Visualization, Validation, Investigation, Formal analysis, Data curation, Conceptualization. **Jack Botting:** Writing – review & editing, Visualization, Validation, Methodology, Investigation, Formal analysis. **Inês B. Gomes:** Writing – review & editing, Visualization, Validation, Methodology, Investigation, Formal analysis, Conceptualization. **Maria J. Saavedra:** Writing – review & editing, Visualization, Validation, Supervision, Methodology, Formal analysis, Conceptualization. **Lúcia C. Simões:** Writing – review & editing, Visualization, Validation, Supervision, Methodology, Data curation, Conceptualization. **Jun Liu:** Writing – review & editing, Visualization, Validation, Software, Resources, Methodology, Formal analysis, Conceptualization. **Manuel Simões:** Writing – review & editing, Visualization, Validation, Supervision, Software, Resources, Project administration, Funding acquisition, Formal analysis, Conceptualization.

Declaration of competing interest

The authors declare that they have no known competing financial interests or personal relationships that could have appeared to influence the work reported in this paper.

Data availability

The authors declare that materials described in the manuscript, including all relevant raw data, will be freely available to any researcher wishing to use them for noncommercial purposes, without breaching participant confidentiality.

References

Afonso, A.C., Gomes, I.B., Saavedra, M.J., Giaouris, E., Simões, L.C., Simões, M., 2021. Bacterial coaggregation in aquatic systems. Water Res. 196 https://doi.org/10.1016/J.WATRES.2021.117037.

Afonso, A.C., Gomes, I.B., Saavedra, M.J., Simões, L., Simões, M., 2023. Drinking-water isolated *Delftia acidovorans* selectively coaggregates with partner bacteria and facilitates multi-species biofilm development. Sci. Total Environ. 162646 https://doi.org/10.1016/J.SCITOTENV.2023.162646.

Afonso, A.C., Simões, M., Saavedra, M.J., Simões, L., Lema, J.M., Trueba-Santiso, A., 2024. Exploring coaggregation mechanisms involved in biofilm formation in drinking water through a proteomic-based approach. J. Appl. Microbiol. 135, 143. https://doi.org/10.1093/JAMBIO/LXAE143.

Baumeister, W., 2022. Cryo-electron tomography: a long journey to the inner space of cells. Cell 185, 2649–2652. https://doi.org/10.1016/J.CELL.2022.06.034.

Bayoudh, S., Othmane, A., Mora, L., Ben Ouada, H., 2009. Assessing bacterial adhesion using DLVO and XDLVO theories and the jet impingement technique. Coll. Surf. B Biointerf. 73, 1–9. https://doi.org/10.1016/J.COLSURFB.2009.04.030.

Borges, A., Saavedra, M.J., Simões, M., 2012. The activity of ferulic and gallic acids in biofilm prevention and control of pathogenic bacteria. Biofouling 28, 755–767. https://doi.org/10.1080/08927014.2012.706751.

Bos, R., van der Mei, H.C., Meinders, J.M., Busscher, H.J., 1994. A quantitative method to study co-adhesion of microorganisms in a parallel plate flow chamber: basic principles of the analysis. J. Microbiol. Methods 20, 289–305. https://doi.org/10.1016/0167-7012(94)90053-1.

Bos, R., van der Mei, H.C., Busscher, H.J., 1999. Physico-chemistry of initial microbial adhesive interactions – its mechanisms and methods for study. FEMS Microbiol. Rev. 23, 179–230. https://doi.org/10.1111/j.1574-6976.1999.tb00396.x.

Burmølle, M., Ren, D., Bjarnsholt, T., Sørensen, S.J., 2014. Interactions in multispecies biofilms: do they actually matter? Trends Microbiol. https://doi.org/10.1016/j.tim.2013.12.004.

Busscher, H., Bos, R., van der Mei, H., 1995. Initial microbial adhesion is a determinant for the strength of biofilm adhesion. FEMS Microbiol. Lett. 128, 229–234. https://doi.org/10.1111/j.1574-6968.1995.tb07529.x.

Cai, S., Wu, Y., Guillen-Samande, A., Hancock-Cerutt, W., Liu, J., De Camilli, P., 2022. *In situ* architecture of the lipid transport protein VPS13C at ER-lysosome membrane contacts. Proc. Natl. Acad. Sci. U. S. A. 119 https://doi.org/10.1073/PNAS.2203769119/-/DCSUPPLEMENTAL.

Chang, C., Wu, C., Osipiuk, J., Siegel, S.D., Zhu, S., Liu, X., Joachimiak, A., Clubb, R.T., Das, A., Ton-That, H., 2019. Cell-to-cell interaction requires optimal positioning of a pilus tip adhesin modulated by gram-positive transpeptidase enzymes. Proc. Natl. Acad. Sci. U. S. A. 116, 18041–18049. https://doi.org/10.1073/PNAS.1907733116.

Donlan, R.M., 2002. Biofilms: microbial life on surfaces. Emerg. Infect. Dis. 8, 881. https://doi.org/10.3201/eid0809.020063.

Dunstone, M.A., de Marco, A., 2017. Cryo-electron tomography: an ideal method to study membrane-associated proteins. Philos. Trans. R. Soc. Lond. B Biol. Sci. 372 https://doi.org/10.1098/RSTB.2016.0210.

Eboigbodin, K.E., Ojeda, J.J., Biggs, C.A., 2007. Investigating the surface properties of *Escherichia coli* under glucose controlled conditions and its effect on aggregation. Langmuir 23, 6691–6697. https://doi.org/10.1021/LA063404Z.

Elias, S., Banin, E., 2012. Multi-species biofilms: living with friendly neighbors. FEMS Microbiol. Rev. 36, 990–1004. https://doi.org/10.1111/J.1574-6976.2012.00325.X.

Halder, S., Yadav, K.K., Sarkar, R., Mukherjee, S., Saha, P., Haldar, S., Karmakar, S., Sen, T., 2015. Alteration of zeta potential and membrane permeability in bacteria: a study with cationic agents. Springerplus 4, 1–14. https://doi.org/10.1186/S40064-015-1476-7.

Handley, P.S., Harty, D.W.S., Wyatt, J.E., Brown, C.R., Doran, J.P., Gibbs, A.C.C., 1987. A comparison of the adhesion, coaggregation and cell-surface hydrophobicity properties of fibrillar and fimbriate strains of *Streptococcus salivarius*. J. Gen. Microbiol. 133, 3207–3217. https://doi.org/10.1099/00221287-133-11-3207.

Higashi, J.M., Wang, I.W., Shlaes, D.M., Anderson, J.M., Marchant, R.E., 1998. Adhesion of *Staphylococcus epidermidis* and transposon mutant strains to hydrophobic polyethylene - PubMed. J. Biomed. Mater. Res. 39.

Ivanchenko, M.V., Indzhykulian, A.A., Corey, D.P., 2021. Electron microscopy techniques for investigating structure and composition of hair-cell stereociliary bundles. Front. Cell Dev. Biol. 9 https://doi.org/10.3389/FCELL.2021.744248.

Janczuk, B., Chibowski, E., Bruque, J.M., Kerkeb, M.L., Caballero, F.G., 1993. On the consistency of surface free energy components as calculated from contact angles of different liquids: an application to the cholesterol surface. J. Colloid Interface Sci. 159, 421–428. https://doi.org/10.1006/jcis.1993.1342.

Jenkinson, H.F., 1992. Adherence, coaggregation, and hydrophobicity of *Streptococcus gordonii* associated with expression of cell surface lipoproteins. Infect. Immun. 60, 1225–1228. https://doi.org/10.1128/IAI.60.3.1225-1228.1992.

Katharios-Lanwermeyer, S., Xi, C., Jakubovics, N.S., Rickard, A.H., 2014. Mini-review: microbial coaggregation: ubiquity and implications for biofilm development. Biofouling 30, 1235–1251. https://doi.org/10.1080/08927014.2014.976206.

Katsikogianni, M., Missirlis, Y.F., Harris, L., Douglas, J., 2004. Concise review of mechanisms of bacterial adhesion to biomaterials and of techniques used in estimating bacteria-material interactions. Eur. Cells Mater. https://doi.org/10.22203/eCM.v008a05.

Kimkes, T.E.P., Heinemann, M., 2020. How bacteria recognise and respond to surface contact. FEMS Microbiol. Rev. 44, 106–122. https://doi.org/10.1093/femsre/fuz029.

Kolenbrander, P., Palmer, R., Rickard, A., Jakubovics, N., Chalmers, N., Diaz, P., 2006. Bacterial interactions and successions during plaque development. Periodontol 2000. https://doi.org/10.1111/j.1600-0757.2006.00187.x.

Kremer, J.R., Mastronarde, D.N., McIntosh, J.R., 1996. Computer visualization of three-dimensional image data using IMOD. J. Struct. Biol. 116, 71–76. https://doi.org/10.1006/JSBI.1996.0013.

Liu, J., Lin, T., Botkin, D.J., McCrum, E., Winkler, H., Norris, S.J., 2009. Intact flagellar motor of *Borrelia burgdorferi* revealed by cryo-electron tomography: evidence for stator ring curvature and rotor/C-ring assembly flexion. J. Bacteriol. 191, 5026–5036. https://doi.org/10.1128/JB.00340-09.

Lučić, V., Rigort, A., Baumeister, W., 2013. Cryo-electron tomography: the challenge of doing structural biology *in situ*. J. Cell Biol. 202, 407–419. https://doi.org/10.1083/JCB.201304193.

Maiti, N.C., Apetri, M.M., Zagorski, M.G., Carey, P.R., Anderson, V.E., 2004. Raman spectroscopic characterization of secondary structure in natively unfolded proteins: alpha-synuclein. J. Am. Chem. Soc. 126, 2399–2408. https://doi.org/10.1021/JA0356176.

Malatesta, M., 2021. Transmission electron microscopy as a powerful tool to investigate the interaction of nanoparticles with subcellular structures. Int. J. Mol. Sci. 22 https://doi.org/10.3390/IJMS222312789.

Malik, A., Sakamoto, M., Hanazaki, S., Osawa, M., Suzuki, T., Tochigi, M., Kakii, K., 2003. Coaggregation among nonflocculating bacteria isolated from activated sludge. Appl. Environ. Microbiol. 69, 6056–6063. https://doi.org/10.1128/AEM.69.10.6056-6063.2003.

Maquelin, K., Kirschner, C., Choo-Smith, L.P., Van Den Braak, N., Endtz, H.P., Naumann, D., Puppels, G.J., 2002. Identification of medically relevant microorganisms by vibrational spectroscopy. J. Microbiol. Methods 51, 255–271. https://doi.org/10.1016/S0167-7012(02)00127-6.

Melia, C.E., Bolla, J.R., Katharios-Lanwermeyer, S., Mihaylov, D.B., Hoffmann, P.C., Huo, J., Wozny, M.R., Elfari, L.M., Böhning, J., Morgan, A.N., Hitchman, C.J., Owens, R.J., Robinson, C.V., O'Toole, G.A., Bharat, T.A.M., 2021. Architecture of cell-cell junctions *in situ* reveals a mechanism for bacterial biofilm inhibition. Proc. Natl. Acad. Sci. U. S. A. 118 https://doi.org/10.1073/PNAS.2109940118/-/DCSUPPLEMENTAL.

Meng, Q., Gao, Q., Mehrazarin, S., Tangwanichgapong, K., Wang, Y., Huang, Y., Pan, Y., Robinson, S., Liu, Z., Zangiabadi, A., Lux, R., Papapanou, P.N., Guo, X.E., Wang, H., Berchowitz, L.E., Han, Y.W., 2021. *Fusobacterium nucleatum* secretes amyloid-like FadA to enhance pathogenicity. EMBO Rep. 22 https://doi.org/10.15252/EMBR.202152891.

Meyers, R.A., 2006. Infrared spectroscopy in microbiology. In: Naumann, D. (Ed.), Encyclopedia of Analytical Chemistry: Applications, Theory and Instrumentation. John Wiley & Sons, Ltd., pp. 1–32. https://doi.org/10.1002/9780470027318

Min, S.C., Schraft, H., Hansen, L.T., Mackereth, R., 2006. Effects of physicochemical surface characteristics of *Listeria monocytogenes* strains on attachment to glass. Food Microbiol. 23, 250–259. https://doi.org/10.1016/J.FM.2005.04.004.

Morath, S., von Aulock, S., Hartung, T., 2005. Structure/function relationships of lipoteichoic acids. J. Endotoxin Res. 11, 348–356. https://doi.org/10.1179/096805105X67328.

Naumann, D., Helm, D., Labischinski, H., 1991. Microbiological characterizations by FT-IR spectroscopy. Nature 351, 81–82. https://doi.org/10.1038/351081A0.

Neumann, A.W., David, R., Zuo, Y., 2010. Applied surface thermodynamics. In: Focus Surfactants. CRC Press. https://doi.org/10.1016/S1351-4210(11)70090-7.

Niemann, H.H., Schubert, W.D., Heinz, D.W., 2004. Adhesins and invasins of pathogenic bacteria: a structural view. Microbes Infect. https://doi.org/10.1016/j.micinf.2003.11.001.

Nishiyama, K., Ochiai, A., Tsubokawa, D., Ishihara, K., Yamamoto, Y., Mukai, T., 2013. Identification and characterization of sulfated carbohydrate-binding protein from *Lactobacillus reuteri*. PloS One 8, 83703. https://doi.org/10.1371/JOURNAL.PONE.0083703.

Oh, J.K., Yegin, Y., Yang, F., Zhang, M., Li, J., Huang, S., Verkhoturov, S.V., Schweikert, E.A., Perez-Lewis, K., Scholar, E.A., Taylor, T.M., Castillo, A., Cisneros-Zevallos, L., Min, Y., Akbulut, M., 2018. The influence of surface chemistry on the kinetics and thermodynamics of bacterial adhesion. Sci. Rep. 81 (8), 1–13. https://doi.org/10.1038/s41598-018-35343-1.

Ojeda, J.J., Romero-González, M.E., Bachmann, R.T., Edyvean, R.G.J., Banwart, S.A., 2008. Characterization of the cell surface and cell wall chemistry of drinking water bacteria by combining XPS, FTIR spectroscopy, modeling, and potentiometric titrations. Langmuir 24, 4032–4040. https://doi.org/10.1021/LA702284B/SUPPL_FILE/LA702284B-FILE002.PDF.

Peters, B.M., Jabra-Rizk, M.A., O'May, G.A., William Costerton, J., Shirtliff, M.E., 2012. Polymicrobial interactions: impact on pathogenesis and human disease. Clin. Microbiol. Rev. 25, 193. https://doi.org/10.1128/CMR.00013-11.

Rendueles, O., Ghigo, J.M., 2012. Multi-species biofilms: how to avoid unfriendly neighbors. FEMS Microbiol. Rev. https://doi.org/10.1111/j.1574-6976.2012.00328.x.

Rickard, A., Thomas, J., Leach, S., Buswell, C., High, N., Handley, P., 1999. Coaggregation amongst aquatic and oral bacteria is mediated by lectinsaccharide interactions. In: Wimpenny, J., Gilbert, P., Walker, J., Brading, M., Bayston, R. (Eds.), Biofilms: The Good, the Bad and the Ugly. Bioline, Cardiff, pp. 343–354.

Rickard, A., McBain, A., Ledder, R., Handley, P., Gilbert, P., 2003a. Coaggregation between freshwater bacteria within biofilm and planktonic communities. FEMS Microbiol. Lett. 220, 133–140. https://doi.org/10.1016/S0378-1097(03)00094-6.

Rickard, A., Gilbert, P., High, N., Kolenbrander, P., Handley, P., 2003b. Bacterial coaggregation: an integral process in the development of multi-species biofilms. Trends Microbiol. https://doi.org/10.1016/S0966-842X(02)00034-3.

Rodrigues, C., Sousa, C., Lopes, J.A., Novais, Â., Peixe, L., 2020. A front line on *Klebsiella pneumoniae* capsular polysaccharide knowledge: fourier transform infrared spectroscopy as an accurate and fast typing tool. mSystems 5. https://doi.org/10.1128/MSYSTEMS.00386-19.

Romaní, M., Guasch, H., Balaguer, M., 2016. Aquatic Biofilms: Ecology, Water Quality and Wastewater Treatment, Aquatic Biofilms: Ecology, Water Quality and Wastewater Treatment. Caister Academic Press, Norfolk, UK. https://doi.org/10.21775/9781910190173.

Sidhu, M.S., Olsen, I., 1997. S-layers of *Bacillus* species. Microbiology 143 (Pt 4), 1039–1052. https://doi.org/10.1099/00221287-143-4-1039.

Simões, L.C., Simões, M., Oliveira, R., Vieira, M.J., 2007. Potential of the adhesion of bacteria isolated from drinking water to materials. J. Basic Microbiol. 47, 174–183. https://doi.org/10.1002/jobm.200610224.

Simões, L., Simões, M., Vieira, M., 2008. Intergeneric coaggregation among drinking water bacteria: evidence of a role for *Acinetobacter calcoaceticus* as a bridging bacterium. Appl. Environ. Microbiol. 74, 1259–1263. https://doi.org/10.1128/AEM.01747-07.

Simões, M., Simões, L., Vieira, M., 2010. Influence of the diversity of bacterial isolates from drinking water on resistance of biofilms to disinfection. Appl. Environ. Microbiol. 76, 6673–6679. https://doi.org/10.1128/AEM.00872-10.

Sousa, C., Novais, A., Magalhães, A., Lopes, J., Peixe, L., 2013. Diverse high-risk B2 and D *Escherichia coli* clones depicted by Fourier Transform Infrared Spectroscopy. Sci. Rep. 31 (3), 1–8. https://doi.org/10.1038/srep03278.

Sousa, Clara, Silva, L., Grosso, F., Lopes, J., Peixe, L., 2014a. Development of a FTIR-ATR based model for typing clinically relevant *Acinetobacter baumannii* clones belonging to ST98, ST103, ST208 and ST218. J. Photochem. Photobiol. B 133, 108–114. https://doi.org/10.1016/J.JPHOTOBIOL.2014.02.015.

Sousa, C., Silva, L., Grosso, F., Nemec, A., Lopes, J., Peixe, L., 2014b. Discrimination of the *Acinetobacter calcoaceticus-Acinetobacter baumannii* complex species by Fourier transform infrared spectroscopy. Eur. J. Clin. Microbiol. Infect. Dis. 33, 1345–1353. https://doi.org/10.1007/S10096-014-2078-Y.

Spillmann, D., Thomas-Oates, J.E., Van Kuik, J.A., Vliegenthart, J.F.G., Misevic, G., Burger, M.M., Finne, J., 1995. Characterization of a novel sulfated carbohydrate unit implicated in the carbohydrate-carbohydrate-mediated cell aggregation of the marine sponge *Microciona prolifera*. J. Biol. Chem. 270, 5089–5097. https://doi.org/10.1074/JBC.270.10.5089.

Tandavanitj, S., Okutani, K., 1989. The structural investigation of a sulfated polysaccharide produced by a strain of marine *Pseudomonas*. Nippon Suisan Gakkaishi 55, 1845–1849. https://doi.org/10.2331/SUISAN.55.1845.

Tariq, M., Bruijs, C., Kok, J., Krom, B.P., 2012. Link between culture zeta potential Homoge- neity and Ebp in *Enterococcus faecalis*. Appl. Environ. Microbiol. 78, 2282. https://doi.org/10.1128/AEM.07618-11.

Teixeira, P., Lopes, Z., Azeredo, J., Oliveira, R., Vieira, M.J., 2005. Physico-chemical surface characterization of a bacterial population isolated from a milking machine. Food Microbiol. 22, 247–251. https://doi.org/10.1016/J.FM.2004.03.010.

van der Mei, H.C., Bos, R., Busscher, H.J., 1998. A reference guide to microbial cell surface hydrophobicity based on contact angles. Colloids Surf. B Biointerfaces 11, 213–221. https://doi.org/10.1016/S0927-7765(98)00037-X.

Van Gerven, N., Klein, R.D., Hultgren, S.J., Remaut, H., 2015. Bacterial amyloid formation: structural insights into curli biogenesis. Trends Microbiol. 23, 693–706. https://doi.org/10.1016/J.TIM.2015.07.010.

Van Oss, C.J., Ju, L., Chaudhury, M.K., Good, R.J., 1989. Estimation of the polar parameters of the surface tension of liquids by contact angle measurements on gels. J. Colloid Interface Sci. 128, 313–319. https://doi.org/10.1016/0021-9797(89)90345-7.

Vilanova, E., Coutinho, C.C., Mourão, P.A.S., 2009. Sulfated polysaccharides from marine sponges (Porifera): an ancestor cell-cell adhesion event based on the carbohydrate-carbohydrate interaction. Glycobiology 19, 860–867. https://doi.org/10.1093/GLYCOB/CWP059.

Vilanova, E., Santos, G.R.C., Aquino, R.S., Valle-Delgado, J.J., Anselmetti, D., Fernàndez-Busquets, X., Mourão, P.A.S., 2016. Carbohydrate-carbohydrate interactions mediated by sulfate esters and calcium provide the cell adhesion required for the emergence of early metazoans. J. Biol. Chem. 291, 9425. https://doi.org/10.1074/JBC.M115.708958.

Worawattanamateekul, W., Okutani, K., 1992. Isolation and characterization of a sulfated polysaccharide produced by a marine bacterium. Nippon Suisan Gakkaishi 58, 1729–1733. https://doi.org/10.2331/SUISAN.58.1729.

Yang, L., Liu, Y., Wu, H., Høiby, N., Molin, S., Song, Z.J., 2011. Current understanding of multi-species biofilms. In: International Journal of Oral Science. Int J Oral Sci, pp. 74–81. https://doi.org/10.4248/IJOS11027.

Yang, S., Wu, Y., Qu, C., Fein, J.B., He, Y., Huang, Q., Cai, P., 2021. Quantitative analysis of the surficial and adhesion properties of the gram-negative bacterial species *Comamonas testosteroni* modulated by c-di-GMP. Colloids Surf. B Biointerfaces 198. https://doi.org/10.1016/J.COLSURFB.2020.111497.

Zähringer, U., Knirel, Y.A., Lindner, B., Helbig, J.H., Sonesson, A., Marre, R., Rietschel, E.T., 1995. The lipopolysaccharide of *Legionella pneumophila* serogroup 1 (strain Philadelphia 1): chemical structure and biological significance - PubMed. Prog. Clin. Biol. Res. 392.

Zhang, Xinru, Yuan, H., Wang, Y., Guan, L., Zeng, Z., Jiang, Z., Zhang, Xinxin, 2020. Cell surface energy affects the structure of microalgal biofilm. Langmuir 36, 3057–3063. https://doi.org/10.1021/ACS.LANGMUIR.0C00274/ASSET/IMAGES/LARGE/LA0C00274_0002.JPEG.

Zhang, Z., Liu, S., Zhang, S., Li, Y., Shi, X., Liu, D., Pan, Y., 2022. *Porphyromonas gingivalis* outer membrane vesicles inhibit the invasion of *Fusobacterium nucleatum* into oral epithelial cells by downregulating FadA and FomA. J. Periodontol. 93, 515–525. https://doi.org/10.1002/JPER.21-0144.

Zheng, S.Q., Palovcak, E., Armache, J.P., Verba, K.A., Cheng, Y., Agard, D.A., 2017. MotionCor2: anisotropic correction of beam-induced motion for improved cryo-electron microscopy. Nat. Methods 14, 331–332. https://doi.org/10.1038/NMETH.4193.